23rd International Conference
ENGINEERING MECHANICS 2017
Svratka, Czech Republic, 15 – 18 May 2017

DUCTILE FRACTURE CRITERIA IMPLEMENTATION AND CALIBRATION USING THE TENSION–TORSION TESTS

F. Šebek[*], J. Petruška[**], P. Kubík[***]

Abstract: *Ductile fracture calibration needs to be done on the basis of reliable experimental testing. Reliable from the proportional loading path point of view, and the knowledge of crack initiation location too. Tubular specimen was designed and biaxially tested to be used for calibration of phenomenological criterion as well as for the comparison to other tubular biaxially tested specimens from recent literature. Calibrated phenomenological criterion was implemented by developed algorithm to Abaqus using the user subroutine in order to predict the cracking onset. The proportionality of loading path was tracked together with the evolution of state variables through the wall thickness to conclude the applicability of each specimen for a specific loading.*

Keywords: Damage indication, Tubular specimen, Failure initiation, Ductile crack, Plastic deformation.

1. Introduction

Ductile fracture is typical separation mechanism of polycrystalline materials. The loading yields in deformation of the solid which gives rise to stress. The stress rises with elastic deformation until the yield point, after which the inelastic deformation develops (Petruška et al., 2012, 2016). Continuing straining leads to development of plastic deformation (Peč et al., 2016) which is accompanied by the degradation of material physical properties. The process is known as a damage accumulation. The material is not capable to bear any further load in the final stage of damage accumulation, the ductility limit is exhausted, and the material ruptures (Šebek et al., 2014). The ductile fracture is driven by the cumulative intensity of plastic strain

$$\bar{\varepsilon}^{p} = \int_{0}^{t} \sqrt{\frac{2}{3}\dot{\boldsymbol{\varepsilon}}^{p} : \dot{\boldsymbol{\varepsilon}}^{p}}\,\mathrm{d}t \tag{1}$$

where $\dot{\boldsymbol{\varepsilon}}^{p}$ is the tensor of plastic strain rate and t is the time. One of the most influencing quantities is the stress triaxiality (Španiel et al., 2014)

$$\eta = \frac{I_1}{3\bar{\sigma}} \tag{2}$$

where I_1 is the first invariant of the Cauchy stress tensor and $\bar{\sigma}$ is the equivalent von Mises stress. Apart from the stress triaxiality, recent criteria include also Lode angle, or another deviatoric stress parameter, as independent state variable (Kubík et al., 2014; Park and Huh, 2014). The normalized Lode angle is

$$\bar{\theta} = \frac{2}{\pi}\arcsin\left(\frac{27}{2}\frac{J_3}{\bar{\sigma}^3}\right) \tag{3}$$

where J_3 is the third invariant of the deviatoric stress tensor.

[*] Ing. František Šebek, PhD.: Institute of Solid Mechanics, Mechatronics and Biomechanics, Faculty of Mechanical Engineering, Brno University of Technology; Technická 2896/2; 616 69, Brno; CZ, sebek@fme.vutbr.cz

[**] Prof. Ing. Jindřich Petruška, PhD.: Institute of Solid Mechanics, Mechatronics and Biomechanics, Faculty of Mechanical Engineering, Brno University of Technology; Technická 2896/2; 616 69, Brno; CZ, petruska@fme.vutbr.cz

[***] Ing. Petr Kubík, PhD.: Institute of Solid Mechanics, Mechatronics and Biomechanics, Faculty of Mechanical Engineering, Brno University of Technology; Technická 2896/2; 616 69, Brno; CZ, kubik.p@fme.vutbr.cz

2. Experimenting and modelling

Fracture tests must be realized in order to calibrate a fracture model. Very important is the crack initiation location as well. Specimens used in calibration of fracture models may have different geometries and may be loaded uniaxially or biaxially to achieve one specific or variety of stress states. The basic experiments were the tensile tests of smooth (6 mm diameter) and notched (R5, R2.5 and R1.2) cylindrical specimens of AISI 1045 carbon steel. Zwick Z050 testing machine with the test speed of 2 mm/min was used. Biaxial tests of Notched Tube (NT) specimens were realized too. The circumferential notch with notch radius R3 was situated on the outer surface. The outer radius in the notch was 4.5 mm and the inner radius of straight hole was 3.5 mm, so the wall thickness was 1 mm in the notch. A pin was put into the shoulder with hole to prevent unwanted deformation during mounting into grips. MTS Bionix 370.02 testing machine was used for biaxial loading. The loading combination may be described by the ratio of axial to torsional movements of testing machine. Loading combinations L = 0, 0.5, 1 and ∞ mm/rad were chosen.

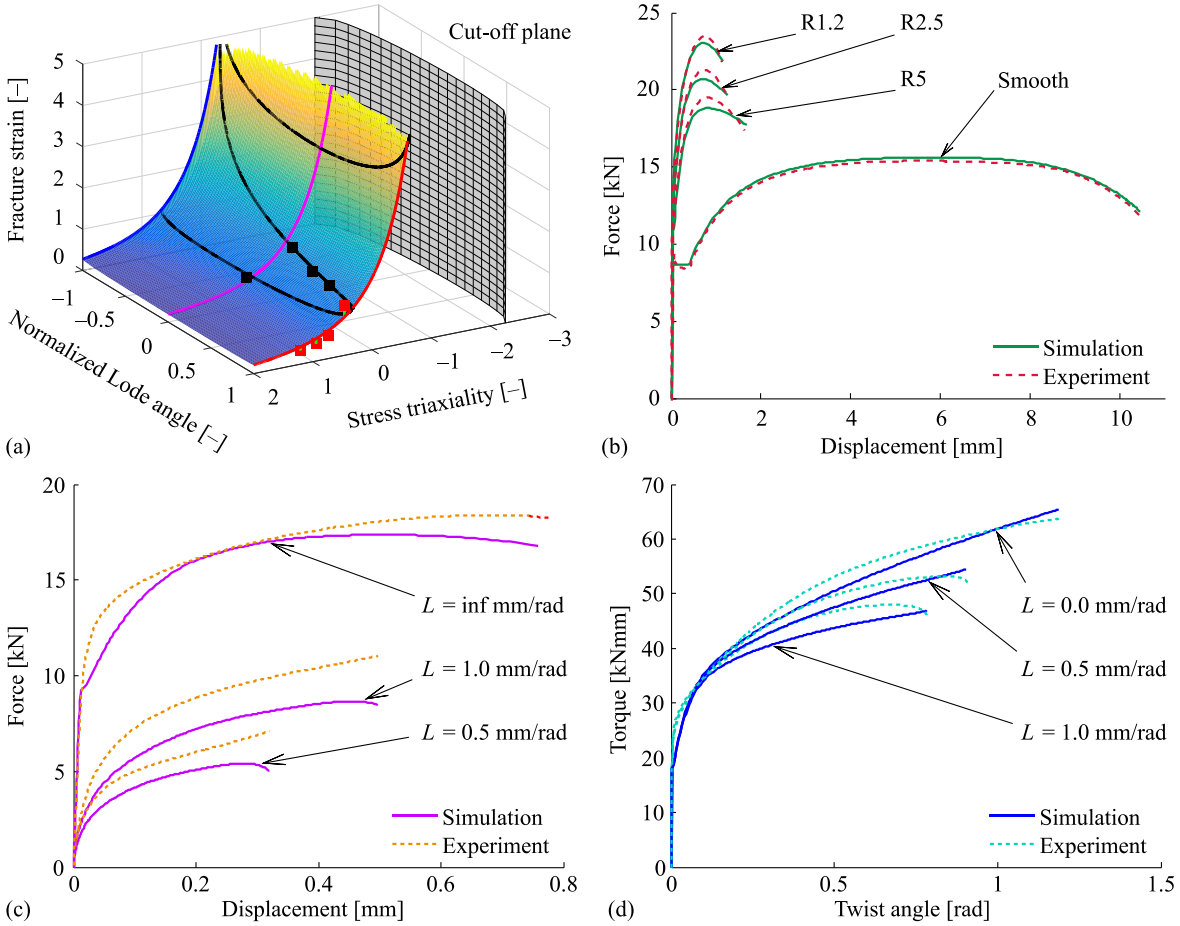

Fig. 1:a) Calibrated Extended Mohr–Coulomb criterion; b) force–displacement responses of round bars; c) force–displacement responses of tubes; d) torque–twist angle responses of tubes.

The von Mises plasticity with isotropic hardening and associated flow rule was adopted. The multi-linear flow curve was calibrated using the tensile smooth round bar (Fig. 1b). Simulations of other tests were carried out (Fig. 1b, c, d) in order to calibrate the Extended Mohr–Coulomb criterion (Bai and Wierzbicki, 2010). It was chosen for the prediction of initiation locations, as described further. The criterion was calibrated with constants 0.2464 and 753.708 MPa and it is depicted in Fig. 1a.

3. Simulations of tension–torsion tests

Tension–torsion specimens create a group of universal specimens because of varying the stress state by changing the loading combination. This chapter deals with comparison of selected four specimens. Those were Double Notched Tube (DNT) (Barsoum and Faleskog, 2007), Modified Lindholm (ML) (Gao et al., 2011), NT (used for calibration) and Tubular Tension–Torsion (TTT) specimen (Papasidero et al., 2014).

First, the torsion was examined. The initiation locations were in the notch roots of all specimens on the outer surfaces (Fig. 2). There were two initiation locations in case of ML and TTT specimens which is not desired (Fig. 2b, d). Note that there is no scale between the geometrical models, therefore the size should be derived from real dimensions.

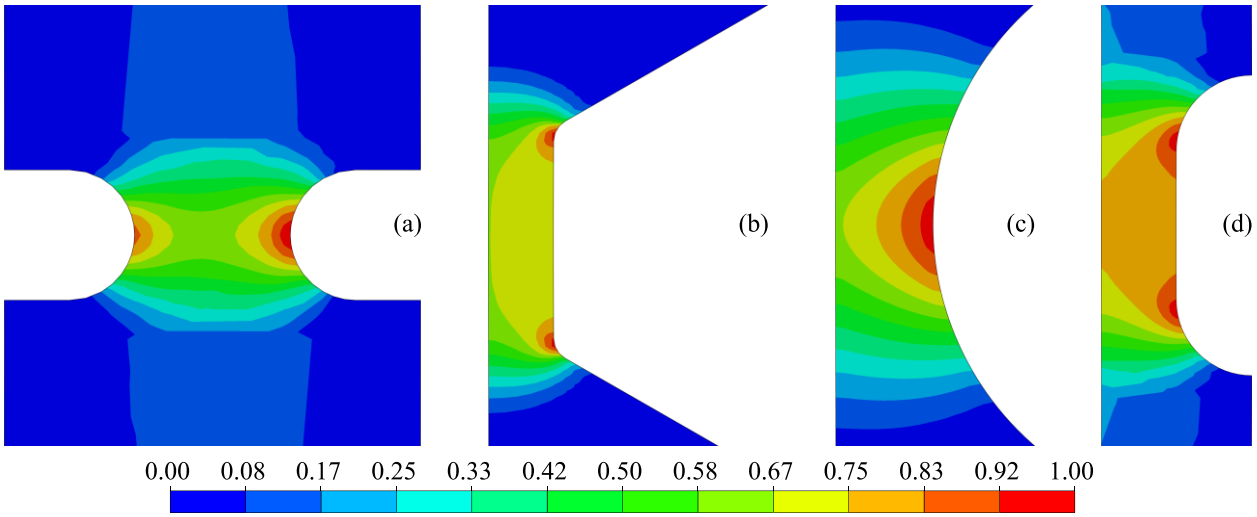

Fig. 2: Damage contours for torsion and (a) DNT; (b) ML; (c) NT; (d) TTT.

The initiation locations for loading combination with prevailing torsion were similar to those obtained for torsion. The worst distribution of state variables through the normalized thickness was in the case of DNT specimen (Fig. 3). It might be caused by very sharp notches and a thin wall.

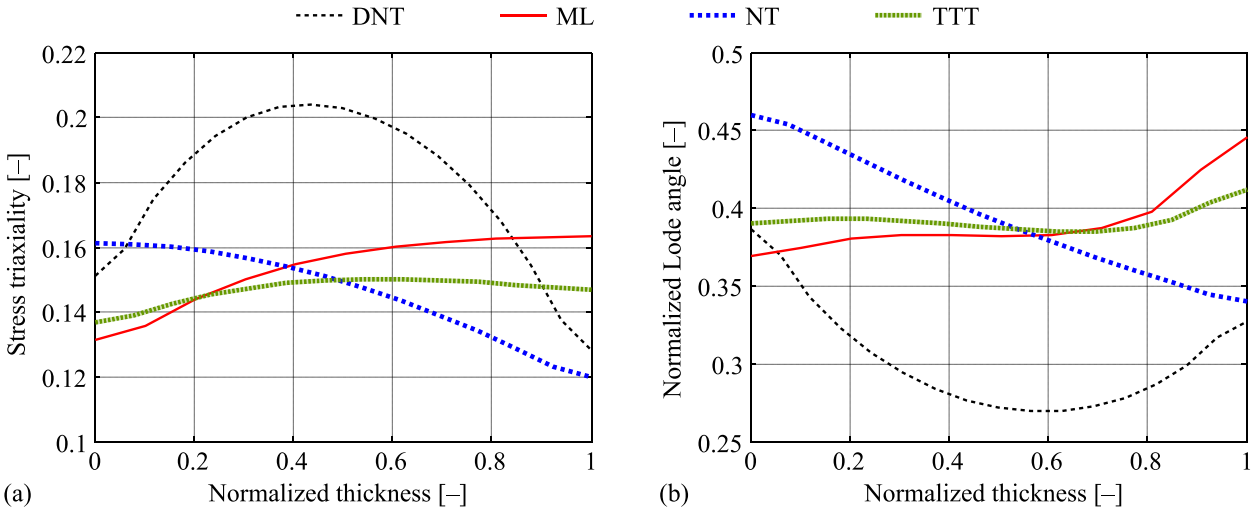

Fig. 3: Distribution of state variables for prevailing torsion along the normalized thickness: a) stress triaxiality; b) normalized Lode angle.

The crack initiated nearby the center of the wall thickness in case of DNT specimen for prevailing tension. The locations of ML and TTT specimens were just beneath the inner surfaces at the central prismatic parts. The initiation location was in the center of the wall at NT specimen for the prevailing tension loading combination. Generally, the initiation was located to one specific site for each specimen. Moreover, it was concentrated to the prismatic part, which is desirable. The stress state reached by DNT specimen was distinctly different than those obtained by the others (Fig. 4). Moreover, the others were closer to the proportional loading that DNT. Therefore, the fracture strain was also noticeably smaller because of much higher stress triaxiality due to the sharp notch radii. The situation was basically similar for tension compared to the prevailing tension.

Generally, the initiation locations of DNT and NT specimens were moving from the outer surface to the center of the wall thickness with increasing tension component of tension–torsion loading. The locations in case of ML and TTT moved from the outer surface to the inner at first, and then to the wall center. The proportionality of loading paths was globally comparable and satisfactory for ductile fracture calibration.

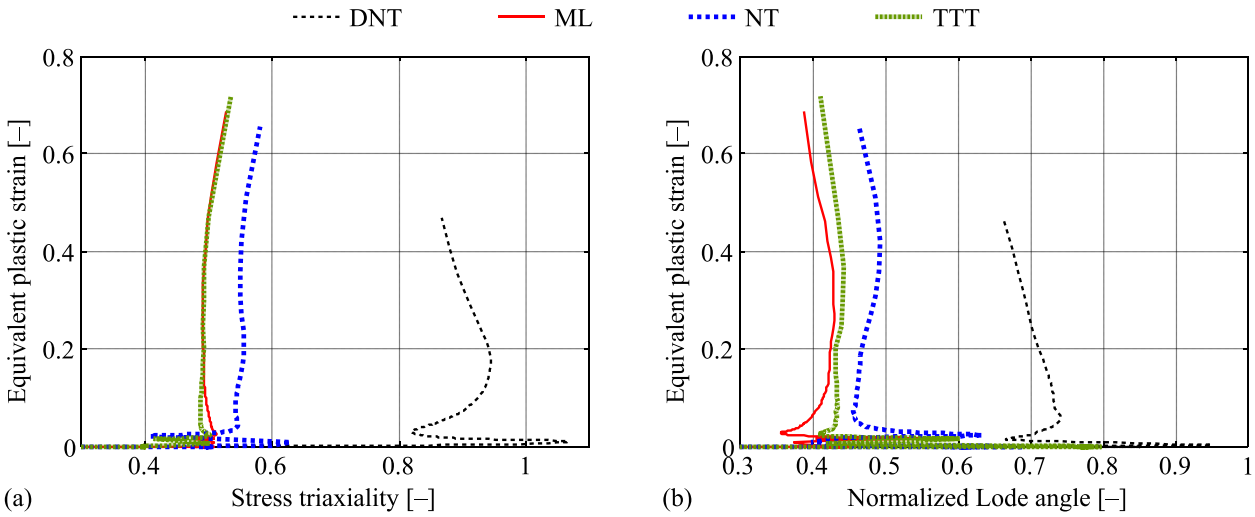

Fig. 4: Equivalent plastic strain for prevailing tension: a) stress triaxiality; b) normalized Lode angle.

4. Conclusions

The experimental testing on designed tension–torsion specimen was conducted and the fracture criterion was calibrated. The criterion was implemented into the commercial software using user subroutine, and it was applied to other tubular specimens from literature, which could be also used for ductile fracture calibration. Generally, ML and TTT behaved similarly as NT, while DNT specimen was noticeably different. The difference was primarily caused by the geometry with double notches of sharp radii. DNT and NT specimens had naturally the fracture initiation locations in one specific cross-section in axial plane of symmetry independently on the loading, which is very good.

Acknowledgement

This work is an output of project NETME CENTRE PLUS (LO1202) created with financial support from the Ministry of Education, Youth and Sports under the „National Sustainability Programme I“.

References

Bai, Y. and Wierzbicki, T. (2010) Application of extended Mohr–Coulomb criterion to ductile fracture. International Journal of Fracture, 161, pp. 1-20.

Barsoum, I. and Faleskog, J. (2007) Rupture mechanisms in combined tension and shear—Experiments. International Journal of Solids and Structures, 44, pp. 1768-1786.

Gao, X., Zhang, T., Zhou, J., Graham, S.M., Hayden, M. and Roe, C. (2011) On stress-state dependent plasticity modeling: Significance of the hydrostatic stress, the third invariant of stress deviator and the non-associated flow rule. International Journal of Plasticity, 27, pp. 217-231.

Kubík, P., Šebek, F., Petruška, J., Hůlka, J., Růžička, J., Španiel, M., Džugan, J. and Prantl, A. (2014) Calibration of selected ductile fracture criteria using two types of specimens. Key Engineering Materials, 592-593, pp. 258-261.

Papasidero, J., Doquet, V. and Mohr, D. (2014) Determination of the effect of stress state on the onset of ductile fracture through tension-torsion experiments. Experimental Mechanics, 54, pp. 137-151.

Park, N. and Huh, H. (2014) Prediction of fracture strains for DP980 steel sheets using a modified Lou–Huh ductile fracture criterion. Key Engineering Materials, 626, pp. 347-352.

Peč, M., Kubík, P., Šebek, F., Návrat, T. and Petruška, J. (2016) Modeling of the blast load effects in explicit dynamics, in: Engineering mechanics 2016, Svratka, pp. 442-445.

Petruška, J., Návrat, T. and Šebek, F. (2012) A new model for fast analysis of leveling process. Advanced Materials Research, 586, pp. 389-393.

Petruška, J., Návrat, T., Šebek, F. and Benešovský, M. (2016) Optimal intermeshing of multi roller cross roll straightening machine, in: AIP Conference Proceedings, 1769, pp. 120002-1-120002-4.

Šebek, F., Kubík, P. and Petruška, J. (2014) Localization problem of coupled ductile failure models compared to uncoupled ones, in: Engineering mechanics 2014, Svratka, pp. 632-635.

Španiel, M., Prantl, A., Džugan, J., Růžička, J., Moravec, M. and Kuželka, J. (2014) Calibration of fracture locus in scope of uncoupled elastic–plastic-ductile fracture material models. Advances in Engineering Software, 72, pp. 95-108.